

AUTHOR QUERIES

AUTHOR PLEASE ANSWER ALL QUERIES

PLEASE NOTE: We cannot accept new source files as corrections for your paper. If possible, please annotate the PDF proof we have sent you with your corrections and upload it via the Author Gateway. Alternatively, you may send us your corrections in list format. You may also upload revised graphics via the Author Gateway.

AQ:1 = Please provide the expansion for the acronyms IPK and CAD.

AQ:2 = Author: Please confirm or add details for any funding or financial support for the research of this article.

AQ:3 = The in-text citations of Figs. 6 and 7 are out of order. Please update the in-text citations.

AQ:4 = Please provide the author names, publisher name, and publisher location for Ref. [1].

AQ:5 = Current affiliation in the biographies of Leon Chao, Julian Stirling, and David Newell do not match the First Footnote. Please check and correct where needed.

AQ:6 = Please provide the year of completion when the author David Newell received the Ph.D. degree.

AQ:7 = Please provide the location for Leader of the Fundamental Electrical Measurements Group and Fundamental Electrical Measurement Group.

The Design and Development of a Tabletop Kibble Balance at NIST

Leon Chao¹, Frank Seifert, Darine Haddad, *Member, IEEE*, Julian Stirling, David Newell, and Stephan Schlamminger

Abstract—On November 16, 2018, the 26th General Conference on Weights and Measures voted unanimously to revise the International System of Units from a system built on seven base units to one built on seven defining constants and will officially become effective on May 20, 2019, or World Metrology Day. More specifically, the unit of mass, the kilogram, will be realized via a fixed value of the Planck constant h and a Kibble balance (KB) serves as one method of achieving this. Over the past few decades, national metrology institutes around the world have developed KBs, the majority aimed at realizing the unit of mass at the 1-kg level with uncertainties on the order of a few parts in 10^8 . However, upon fixing the Planck constant, mass can be directly realized at any level, deeming the kilogram only a historically unique benchmark. At the National Institute of Standards and Technology, a tabletop-sized Kibble balance (KIBB-g1) designed to operate at the gram-level range with uncertainties on the order of a few parts in 10^6 is currently under development.

Index Terms—Kibble balance (KB), mass metrology, precision engineering design.

I. INTRODUCTION

THE maximum permitted uncertainties for International Organization of Legal Metrology (OIML) class E₁ calibration weights ranging from 1 to 10 g are on the order of a few micrograms, limited by the accrued uncertainties associated with repeatability of the balances used within the traceability chain to the IPK and the stability of the artifacts [1]. With the revised International System of Units, mass can be directly realized at any scale point (i.e., milligram, gram, kilogram, etc.) [3]. Instrument manufacturers and pharmaceutical companies have shown interest in directly measuring small masses and a tabletop Kibble balance (KB) capable of realizing mass with the same level of uncertainties associated with a set of calibration weights can replace the need for such a set. Operating at this level of relative uncertainty also removes the demand for quantum electrical standards, gravimeters, and high-vacuum environments required in more accurate KBs. Here, as an extension of [2], we describe the design and development of KIBB-g1, or (KIB)ble (B)alance at the (g)ram level, version (1), aimed at achieving uncertainties on the order of a few micrograms. The final results show promise and set

a foundation for future work in generating a full uncertainty budget.

II. THEORY OF A KIBBLE BALANCE

Even though a KB might appear functionally similar to an equal-arm beam balance, a significant difference exists. A conventional beam balance makes relative measurements, comparing the weight an object to that of a calibrated mass. A KB, however, makes absolute measurements, comparing the weight of an object to a frequently calibrated electromagnetic force determined by electrical quantities. The experiment involves two modes of operation, velocity mode, and force mode. Velocity mode is based on the principle of Faraday's law of induction. A coil (wire length L) is moved at a velocity v through a magnetic field (flux density B) so that a voltage V is induced. The induced voltage is related to the velocity through the flux integral BL

$$V = BLv. \quad (1)$$

Force mode is based on Lorentz forces. The gravitational force on a mass m is counteracted by an upward electromagnetic force F generated by the now current-carrying coil in a magnetic field

$$F = BLI = mg \quad (2)$$

where g is the local gravitational acceleration and I is the current in the coil.

By combining (1) and (2), canceling out the BL factor common to both equations, and rearranging the variables, expressions for electrical and mechanical power are equated and a solution for mass is obtained

$$VI = mgv \implies m = \frac{VI}{gv}. \quad (3)$$

The above-mentioned equation relates mechanical power to electrical power and provides a means to relate mass to electrical quantities. The relationship equates “virtual” power, in the sense that the factors of each product, V and I or mg and v , are not measured simultaneously but separately in the two modes. The “power” only exists virtually, i.e., as a mathematical product.

Since KIBB-g1 strives for relative uncertainties on the order of a few parts in 10^6 , the Planck constant only makes a subtle appearance as the means for absolutely calibrating the hardware associated with the electrical quantities.

Manuscript received July 13, 2018; revised December 26, 2018; accepted February 1, 2019. The Associate Editor coordinating the review process was Djamel Allal. (*Corresponding author: Leon Chao.*)

The authors are with the National Institute of Standards and Technology, Gaithersburg, MD 20899 USA (e-mail: leon.chao@nist.gov).

Color versions of one or more of the figures in this paper are available online at <http://ieeexplore.ieee.org>.

Digital Object Identifier 10.1109/TIM.2019.2901550

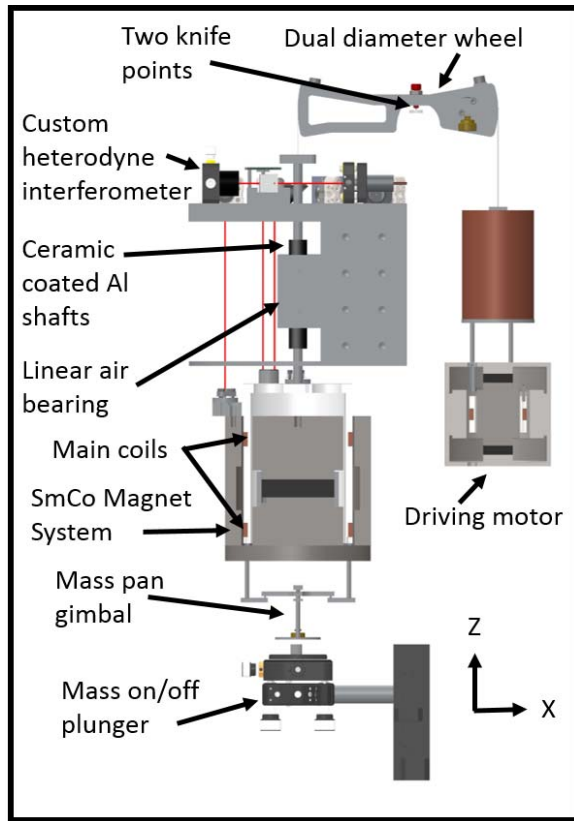


Fig. 1. CAD rendering of the KIBB-g1 KB. Structural components have been hidden for clarity. Cross-sectional views of both magnets/coils are shown. The MMS is everything to the left of the knife points and the CMS to the right.

III. DESIGN OVERVIEW

A. Mechanical

The KIBB-g1 KB was designed with the intention of providing industrial laboratories with the capability to directly realize mass units at the gram level on site. With this in mind, we set out five design goals as follows.

- 1) Form factor: “tabletop” sized instrument.
- 2) Cost: < 50000 USD.
- 3) Nominal values: between 1 and 10 g.
- 4) Relative uncertainties: $\approx 10^{-6}$.
- 5) Convenience: operates in air (no vacuum required).

KIBB-g1 measures 57 cm tall and 30 cm in diameter and is designed such that the “main mass side” (MMS) contains all the components relevant to velocity and force mode while the “counter mass side” (CMS) serves as a driving motor. For a detailed description of KB theory and design (see [4]).

Starting from the top of the balance as shown in Figs. 1 and 2, a dual-diameter truncated wheel pivots about a two-point contact, essentially forming a line contact, which we will commonly refer to as the “knife points.” The two pivot points are commercially available nonmagnetic Niva Alloy¹ points and each rests on a polished sapphire disk.

¹Certain commercial equipment, instruments, and materials are identified in this paper in order to specify the experimental procedure adequately. Such an identification is not intended to imply recommendation or endorsement by the National Institute of Standards and Technology nor is it intended to imply that the materials or equipment identified are necessarily the best available for the purpose.

The simple design of the two knife points essentially provides a straight line contact without the need for manufacturing a precision knife edge.

The truncated wheel looks like a beam but effectively behaves as a wheel. The prescribed motion of the hanging coils along the z -axis is constrained by the rotation of the wheel about the y -axis. The MMS beam arc has a smooth, curved surface with a radius 1.4 times that of the CMS arc where both arcs are concentric. This radius mismatch allows for increased space on the MMS without increasing the form factor of the entire apparatus. Each knife-point is rigidly attached to the end of a screw inserted through the center of the balance beam. Adjusting the depth of each screw allows aligning the rotational degree of freedom (DOF) about the x -axis and translational DOF in the z -axis. This is critical for adjusting the location of the truncated wheel’s center of gravity as well as aligning its geometric center to the rotation center of the knife points.

The MMS electromagnet system consists of two coils with 3253 turns and mean diameter of 73 mm each wound from magnet wire with a diameter of 0.06 mm. The MMS permanent magnet is comprised of a single SmCo magnet disk, the magnetic flux of which is guided by a mild steel yoke. The system is designed such that the magnetic flux is guided radially through the two air gaps for interaction with the two coils. The magnetic flux density through the air gaps is measured to be about 0.4 T.

The coil is rigidly connected to two parallel ceramic coated aluminum shafts and is suspended from the MMS of the beam via a titanium wire. One of the parallel shafts is guided by an air bearing operating at about 240 kPa above the atmosphere. The original design included air bearings for both shafts but the parallelism alignment proved difficult for overcoming the effects of overconstraining. Two shielding plates were bolted above and below the air bearing to reduce the noise from the exhaust. We conducted a force mode measurement with varying input pressures ranging from 240 to 700 kPa, and through higher pressures resulted in an increase in noise, the overall mass determination for each pressure level was consistent. In principle, the air exhaust is a constant offset force common in both the mass ON and mass OFF states during force mode. A vertical tube is implemented to shield the laser paths from small refractive index fluctuations caused by the exhaust air. The lab temperature, humidity, and pressure fluctuations have been measured by an environmental sensor placed next to the magnet for buoyancy and refractive index corrections and the effect of each contributes relatively less than 1×10^{-6} . Suspended from the bottom of the coil is a mass pan gimbal and a piston loads and unloads the test mass.

The CMS consists of a small coil mounted below a copper tube (a dead mass to account for the mass on the MMS), suspended by two filaments of the same wire as the MMS. Small NdFeB magnets interact with the copper tube and serve as eddy current dampers for suppressing the pendulum modes of the CMS hanging assembly. The CMS coil hangs inside a closed-circuit NdFeB/mild steel magnet system.

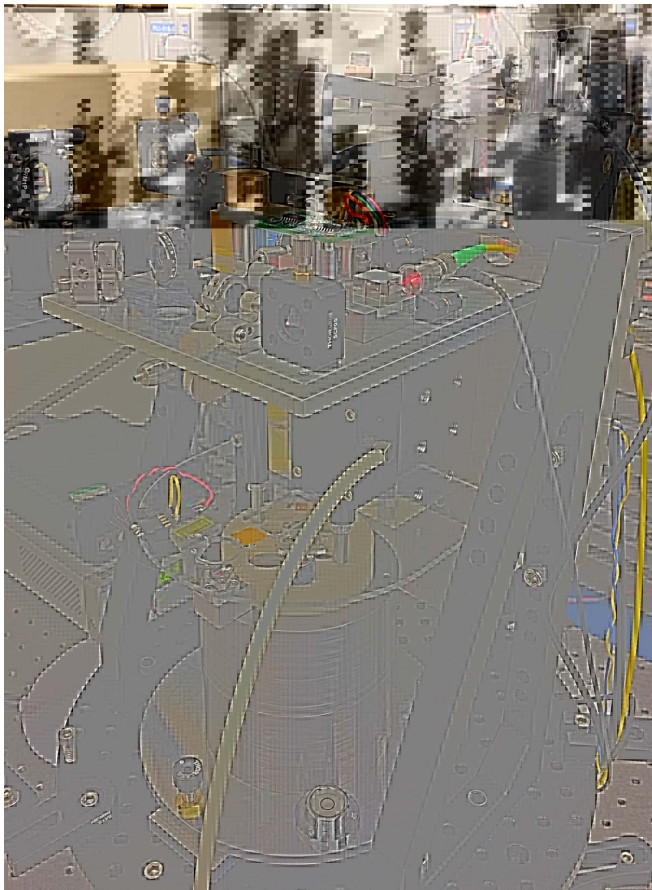


Fig. 2. Photograph of KIBB-g1. White hose for air bearing supply.

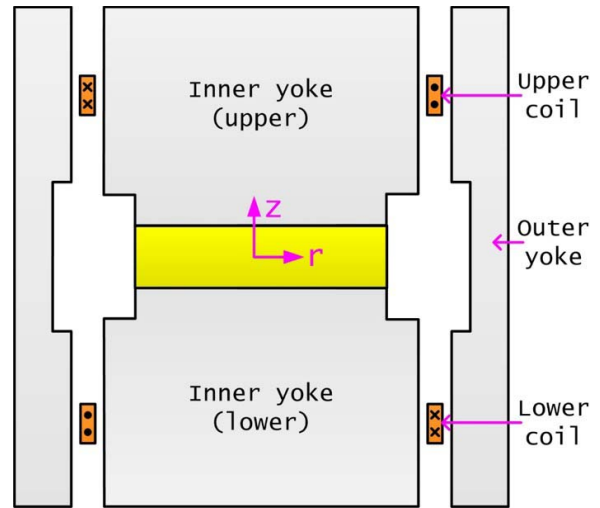


Fig. 3. Cross-sectional representation of the magnet system. Two coils wound on the same former are connected in series opposition. Each coil has 3253 windings. Two halves of the outer yoke have been simplified to a single sleeve.

a PCI-6251 DAQ. In velocity mode, the induced voltage is measured with an Agilent 3458A voltmeter and in force mode, the full voltage drop produced by the weighing current traversing a Fluke 742A 1-k Ω calibrated resistor is measured. All measurement and timing triggers are controlled by a PXI 7831R field-programmable gate array (FPGA). A global positioning system receiver producing a 10-MHz signal serves as the timing source for both the FPGA and TIAs.

161 **B. Optical**

162 A dual frequency 2.83-MHz Zeeman-split laser is used as
 163 the source for the Michelson heterodyne interferometer for
 164 measuring and controlling the displacement of the main coil
 165 along Z . The measurement laser beam of the interferometer
 166 projects onto a flat mirror mounted centered on the top surface
 167 of the coil former adjustable in angle about X and Y . Because
 168 the angular DOF of the coil is constrained by the air bearings,
 169 a simple flat mirror was chosen instead of a retroreflector. The
 170 reference arm projects onto a similar mirror system mounted
 171 to the top edge of the magnet. This location was chosen to
 172 minimize the optical path difference between the two arms and
 173 for common mode rejection of mechanical vibration between
 174 the coil and magnet. The interferometer signals are read
 175 through two Carmel Instruments time interval analyzers (TIA).
 176 One TIA serves as a continuous position and time readout,
 177 whereas the second TIA serves as the measurement readout
 178 for velocity only when triggered. A horizontal displacement
 179 sensor (HDS) is comprised of a separate laser beam which
 180 reflects off a corner cube mounted off-center of the coil former
 181 onto a 2-D position sensor for monitoring minute parasitic
 182 X and Y motions of the coil during the velocity trajectory
 183 and as an aid for aligning the trajectory to gravity.

184 **C. Electrical**

185 The KIBB-g1 coils are connected to a custom built 26-bit
 186 current source through a relay box ultimately controlled by

187 **D. Magnetic**

188 The KIBB-g1 magnet system employs a single SmCo disk
 189 measuring 12.7 mm in height and 50.8 mm in diameter as
 190 the source of the magnetic circuit. Two nearly identical mild
 191 steel cylinders sandwich the magnet and are concentrically
 192 constrained by an aluminum sleeve as shown in Fig. 3. These
 193 three components make up the inner yoke. Two symmetric
 194 tubes made from the same steel are stacked and locked to
 195 each other via three dowel pins and serve as the outer yoke
 196 assembly. Both the inner and outer yoke assemblies are bolted
 197 to an aluminum base plate capable of tip, tilt, and vertical
 198 translation.

199 The upper and lower 7.6-mm-wide and 35.6-mm-tall air
 200 gaps contain the radial magnetic field and are designed to
 201 guide linearly increasing or decreasing magnetic flux densities
 202 with respect to Z as shown in Figs. 4 and 5. Thus, in principle,
 203 the combined magnetic flux density curve is uniform in the
 204 neighborhood of $Z = 0$.

205 The original design of the magnet utilized a monolithic
 206 tube as the outer yoke. However, due to manufacturing and
 207 assembly procedure asymmetries of both the magnet and the
 208 coils, the combined field profile was measured to have a
 209 0.075-Tm/mm slope. A sloped profile, especially at the weigh-
 210 ing position, is undesirable because the mass determinations
 211 are highly sensitive to small deviations about the weighing
 212 position. In attempt to achieve a flat spot in the profile,
 213 a new outer yoke was fabricated as two separate pieces such
 214 as shown in Fig. 3.

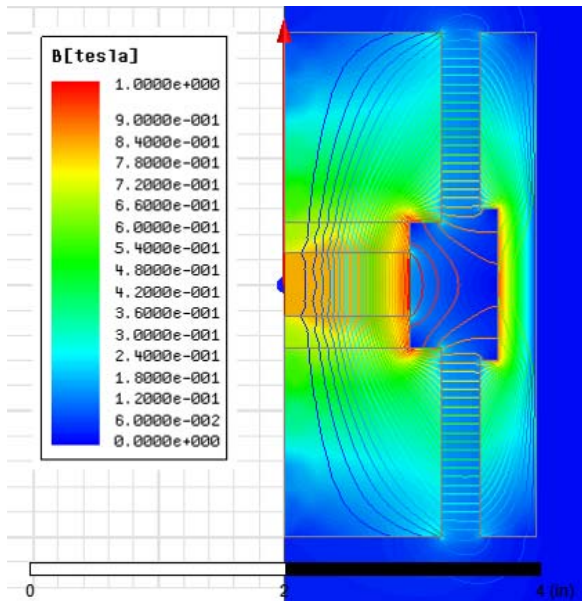


Fig. 4. Finite element simulation of the magnetic flux density through the top and bottom air gaps of half the magnet. The field where the coil resides in weighing mode is approximately 0.4 T.

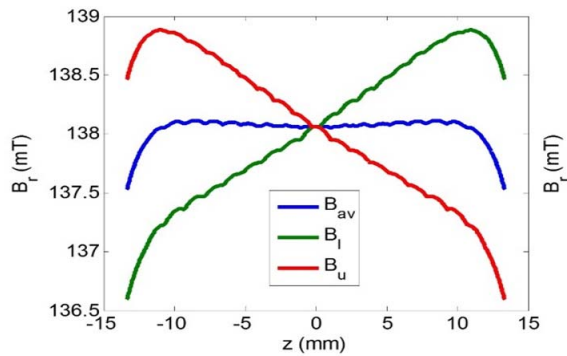


Fig. 5. Theoretical magnetic flux density profile of the upper air gap (B_u), the lower air gap (B_l), and the average of the two (B_{av}) versus vertical position of the coil Z . The MMS coil is comprised of two individual coils connected in series opposition so the measured profile should reflect the shape of B_{av} with a local minimum at $Z = 0$.

that the assembly procedure would be completely symmetric and no yoke pieces would be magnetized more than once. Another attempt was altering the reluctance of the bottom half of the outer yoke with an external magnetic field. Neither attempt influenced the field enough to achieve a uniform profile section. To truly achieve a flat field near $Z = 0$, we had to shim the height of the inner yoke assembly by 2-mm relative to the outer yoke. This led to the most recent magnetic field profile measured in Fig. 7 where the slope is less than 0.004 Tm/mm or in relative terms $2.3 \times 10^{-8}/\mu\text{m}$ near $Z = 0$. The balance controls are typically able to hold weighing position at $Z = 0 \pm 0.5 \mu\text{m}$.

A drawback of the open top/bottom magnet system design is the leakage of the magnetic flux near the unguided regions. Therefore, any test masses will experience a systematic force from the stray magnetic field and its gradient.

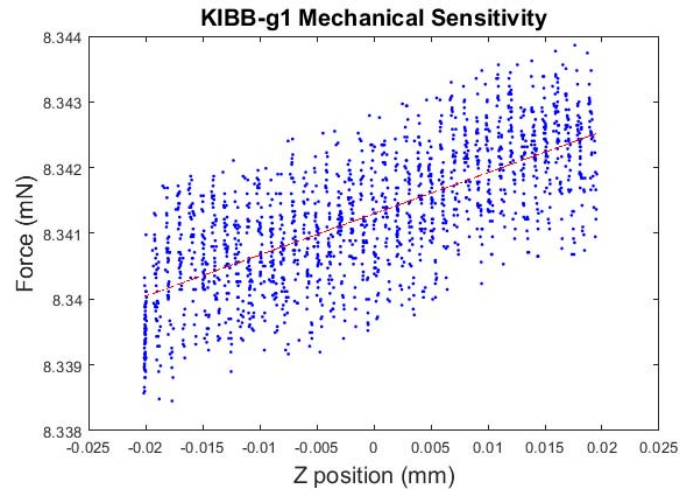


Fig. 6. Measured data of mechanical balance sensitivity between $Z = -0.02 \text{ mm}$ and $Z = 0.02 \text{ mm}$. The force change as a function of Z position is about $0.05 \mu\text{N}/\mu\text{m}$.

The mass pan hangs approximately 50 mm below the bottom surface of the magnet. Thus, for example, an OIML class E₂ 10-g stainless steel mass would experience a force equivalent of a 12-mg mass due to the magnetic susceptibility of the material. A field cancellation procedure of adding a 5-DOF adjustable magnet underneath the mass pan to negate the field at the mass location has proven successful and, in principle, can reduce the magnetic field gradient to zero. However, a strong magnet placed near the mass pan is cumbersome for development purposes so that we have chosen to complete our measurements with masses made from copper for which the systematic forces are negligible.

IV. SYSTEM ALIGNMENT

To align the KB for measurement, verticality of the balance, the HDS, and the interferometer has to be ensured. The magnet, which can be independently tilted, is aligned to be vertical using a precision bubble level. The direction of the interferometer and the HDS laser beams are then aligned to be vertical, defined by g , with reference to an alcohol pool. For example, the verticality of the measurement laser of the interferometer has been adjusted to be within $200 \mu\text{rad}$ mainly due to the length of the optical lever permitted by the depth of the laboratory. The trajectory of the coil is made vertical by iteratively adjusting the KB and HDS to align to g .

At the same time, balance sensitivity was adjusted by shifting the center of gravity of the balance wheel. Two threaded brass masses attached to the CMS of the balance beam allowed to translate in X and Z provide means for such adjustments. Balance sensitivity was adjusted and measured to be about $0.05 \mu\text{N}/\mu\text{m}$ (or $5 \text{ nN}/\mu\text{rad}$ with respect to the wheel angle) near the weighing position, depicted by Fig. 6. As stated earlier, our force mode controller typically holds the position of the coil within $0 \pm 0.5 \mu\text{m}$.

V. MEASUREMENT PROCEDURE AND DATA ANALYSIS

Once the above-mentioned alignment procedure is complete, an acrylic dome is placed over the KB to shield the

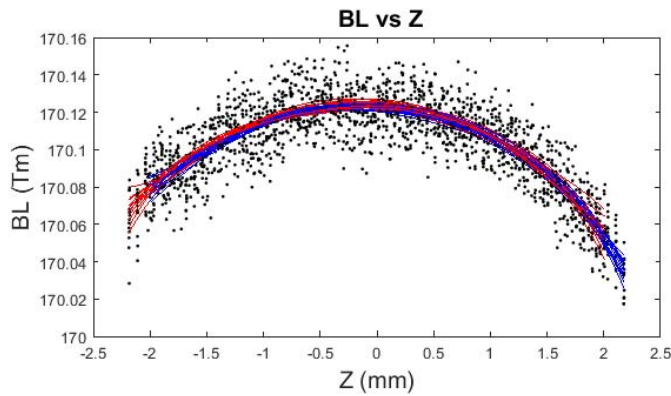


Fig. 7. Example of 29 up/down sweeps superimposed on top of each other in a single-velocity mode data set. BL is plotted against Z position of the coil. Induced voltage is measured at 2 NPLC, 1 mm/s from $Z = -2.2$ mm to $+2.2$ mm. A least squares regression is applied to each sweep.

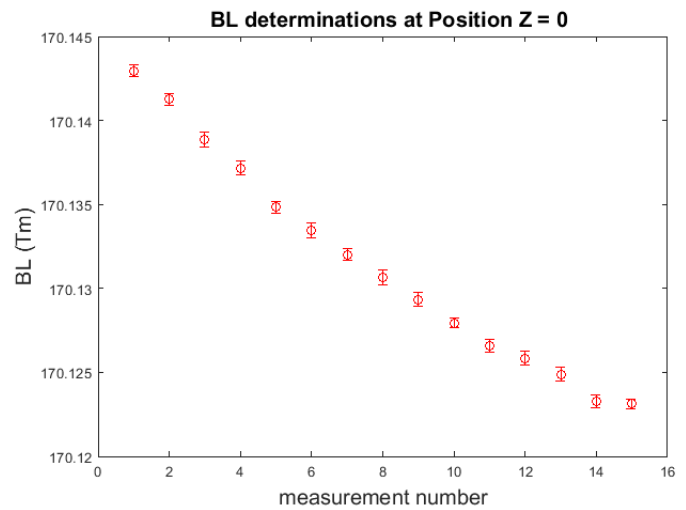


Fig. 8. BL determinations of a full measurement spanning 4.5 h. The relative statistical uncertainty of each determination is on average 2×10^{-6} ($k = 1$). The overlying drift is caused by change of the magnetization due to temperature fluctuations of the laboratory.

274 instrument from air currents caused by the air conditioning in
 275 the laboratory. A small hole in the dome allows passage for the
 276 interferometer laser beam. For the rest of this paper, we will
 277 reference our first attempt at measuring the mass of a copper
 278 cylinder with a value of 10.164780(5) g ($k = 1$, calibrated by
 279 the National Institute of Standards and Technology Mass and
 280 Force Group).

281 Velocity mode operates with the 10-g mass resting on the
 282 mass pan and the KB balanced. The measurement begins
 283 with 14 up and 15 down velocity sweeps with a constant
 284 velocity of 1mm/s while sampling the DVM every 2 power
 285 line cycles (NPLC) or 33 ms. These parameter values were
 286 chosen based on examining the power spectrum of velocity
 287 noise and a separate parametric study between differing NPLC
 288 and velocity values. The FPGA triggers both the sampling of
 289 the TIA and DVM. For example, each voltage measurement
 290 is bracketed by 17 position and time readings where each
 291 set is averaged down to a single position and time. The
 292 velocity during the voltage measurement is determined by
 293 the difference of two consecutive position readings divided
 294 by the sample time. From the voltage and velocity data
 295 pairs, the quotient is calculated, and this is the BL . Each
 296 sweep consists of 60 BL measurements each with its own
 297 Z position ranging between $Z = \pm 2.2$ mm. For this data set,
 298 the least squares regression is performed. Fig. 7 shows the data
 299 of 29 up/down sweeps superimposed on each other. The solid
 300 lines show the polynomial fits. Fig. 8 shows the average of the
 301 BL values extracted from the polynomial fits at $Z = 0$ for
 302 each velocity mode set over the span of 4.5 h. Force mode
 303 measurements occur in between each of these points.

304 After a set of velocity mode measurements, the system
 305 toggles to force mode and the balance is served to $Z = 0$
 306 where the maximum of the BL curve resides. A motorized
 307 translation stage first removes the mass, and the perturbation
 308 due to this process is suppressed with tight control gains.
 309 The balance then undergoes a hysteresis erasing procedure
 310 where the balance follows a decaying sinusoidal trajectory
 311 with an initial amplitude larger than that of the perturbation
 312 caused by the mass removal. This is necessary because the

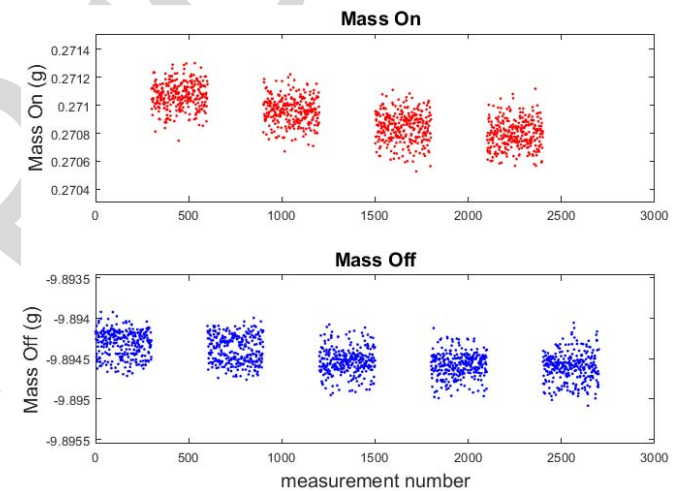


Fig. 9. Example of raw force mode data. Mass imbalance experienced by KIBB-g1 converted from voltage to grams via an interpolated value of BL from bracketing velocity mode measurements is plotted. Four mass on measurements (top). Each cluster is 300 data points taken over 30 s. Five sets of mass off measurements with the same amount of data points and time duration (bottom). The total time required for a weighing mode set is approximately 15 min due to the knife points hysteresis erasing and settling time procedures executed after each mass exchange. Because the distribution seems to have non-Gaussian behavior, we chose not to calculate the standard deviation of the mean for this data set. Thus, all clusters have a relative uncertainty of about 2×10^{-5} ($k = 1$).

313 pivot points are not ideal, frictionless surfaces, and incur a
 314 bias restoring force depending on the direction and amplitude
 315 of the excursion from mass exchanges. Immediately after the
 316 erasing procedure, controller feedback switches to a set of
 317 gains optimized for current noise. After some settling time,
 318 300 current measurements are taken, once every power line
 319 cycle. The process is then repeated for a mass on measurement.
 320 In total, a set of nine mass ON/OFF measurements are taken
 321 per force mode set as shown in Fig. 9. It may be seen that the

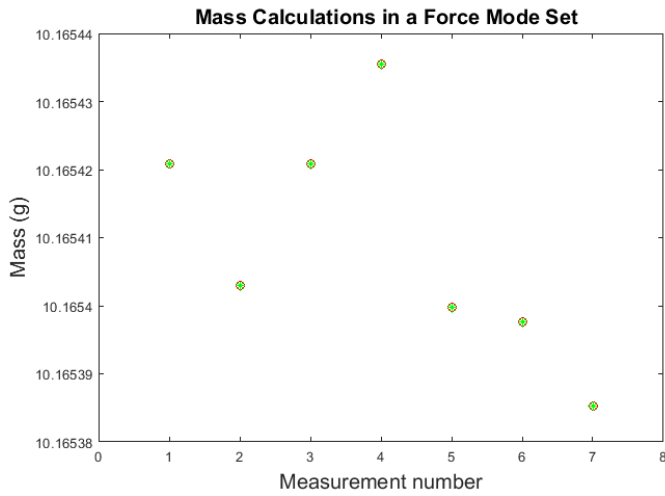


Fig. 10. Example of a set of seven mass calculations in a force mode set. The relative statistical uncertainty of each force mode set is on average 5×10^{-6} ($k = 1$).

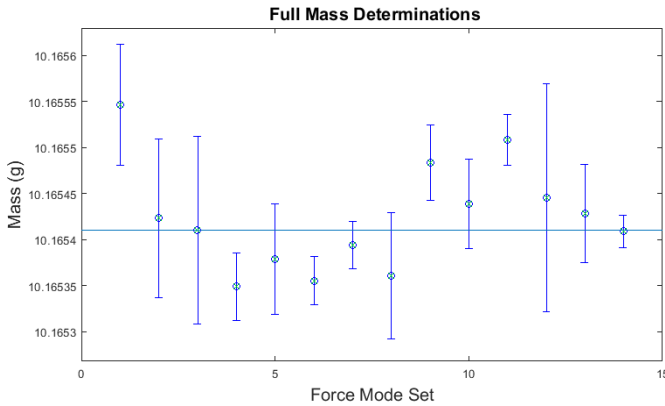


Fig. 11. Example of a set of mass determinations for a copper cylinder with a mass value believed to be 10.164780(5) g. Weighting the data gives a value of 10.16541 g (horizontal line) with a relative statistical uncertainty of 1.2×10^{-6} ($k = 1$). However, the uncertainty needs to be multiplied by an expansion factor of 1.47 (see text).

weighings are asymmetric, that is,

$$|M_{\text{off}}| \neq |M_{\text{on}}|. \quad (4)$$

This is due to mechanical limitations of KIBB-g1, but it is typically best practice to conduct symmetric weighings in a KB experiment.

After the conclusion of the full measurement of 15 velocity mode and 14 force mode sets, the force mode voltage measurements are converted to mass via a linearly interpolated BL value from bracketing velocity mode sets, allowing for seven mass calculations per force mode set as shown in Fig. 10. The first mass calculation is defined as

$$\frac{M_{\text{off}1} - M_{\text{off}2}}{2} - M_{\text{on}1}. \quad (5)$$

The second mass calculation is defined as

$$M_{\text{off}2} - \frac{M_{\text{on}1} - M_{\text{on}2}}{2} \quad (6)$$

and so on. This is to remove any linear time-dependent drift of the magnetic field, usually due to temperature fluctuations, since mass ON and mass OFF are measured at different times. Fig. 9 depicts a typical force mode set. A full measurement set of mass determinations is shown in Fig. 11.

VI. CONCLUSION

KIBB-g1 is still in the prototyping phase. It is an ongoing effort to characterize the apparatus and understand the uncertainties contributing to the accuracy of the measurements. Many of the systematic uncertainties are known to have relative effects at or below 1×10^{-6} , i.e., local acceleration of gravity, laser wavelength, and frequency, refractive index, and buoyancy changes due to environmental fluctuations, resistor, and DVM drift. Temperature, air pressure, and humidity are constantly monitored in the laboratory, and an index of refraction correction for the laser wavelength has been applied. So far, we have been focused on the precision and repeatability of KIBB-g1.

In Fig. 11, 14 data points are represented with their statistical uncertainties. The weighted mean of the data has a relative statistical uncertainty of 1.2×10^{-6} . The χ^2 is 28 for $N - 1 = 13$ DOF, larger than the expected 13. In this case, it is custom to enlarge the individual uncertainties by the Birge ratio, $(\chi^2/(N - 1))^{1/2} = 1.47$. This leads to a relative statistical uncertainty of the mean of 1.7×10^{-6} .

The data in Fig. 11 show a nonstationary pattern. We believe this caused by either choppy mass exchanges or gain changes in the control loop. This is currently under investigation. The pattern in the data is the cause of the larger than expected χ^2 .

The data presented here indicate the precision of KIBB-g1 has uncertainties of about 1.7×10^{-6} on a nominally 10-g mass but the difference between our measured value and the true value is about 6.2×10^{-5} . Thus, we must continue investigating the systematic errors associated with the instrument before an absolute measurement and full uncertainty budget can be completed.

ACKNOWLEDGMENT

The authors would like to thank S. Li for the magnet design, A. Panna for helping with the software development, M. Kraft for the resistor calibration, B. Waltrip and M. Berilla for the current source design, P. Abbott and K. Chesnutwood for the mass calibrations, and J. Pratt and G. Shaw for general support.

REFERENCES

- [1] *Weights of Classes E1, E2, F1, F2, M1, M2, M3, Committee Draft OIML/CD R 111-1 of Edition*, 2004.
- [2] L. Chao, F. Seifert, D. Haddad, S. Schlamminger, "The design and development of a tabletop Kibble balance at NIST," in *Proc. Conf. Precis. Electromagn. Meas.*, Jul. 2018, pp. 1–3.
- [3] D. Haddad *et al.*, "Measurement of the Planck constant at the National Institute of Standards and Technology from 2015 to 2017," *Metrologia*, vol. 54, pp. 633–641, Jul. 2017.
- [4] I. A. Robinson and S. Schlamminger, "The watt or Kibble balance: A technique for implementing the new SI definition of the unit of mass," *Metrologia*, vol. 53, pp. 46–74, Sep. 2016.
- [5] D. Haddad *et al.*, "A precise instrument to determine the Planck constant, and the future kilogram," *Rev. Sci. Instrum.*, vol. 87, May 2016, Art. no. 061301.

336
337
338
339
340
341
342
343
344
345
346
347
348
349
350
351
352
353
354
355
356
357
358
359
360
361
362
363
364
365
366
367
368
369
370
371
372
373
374
375
376
377
378
379
380
381
382
383
384
385
386
387
388
389
390
391
392

AQ:5
393
394
395
396
397
398
399
400
401
402
403



Leon Chao received the B.S. degree in mechanical engineering from the University of Maryland at College Park, College Park, MD, USA, in 2012.

In 2012, he joined the Fundamental Electrical Measurements Group, National Institute of Standards and Technology, Gaithersburg, MD, USA, as a Mechanical Engineer. He is currently with the University of Maryland at College Park, where he is involved in two Kibble balance experiments, NIST-4 and KIBB-g1, while attending graduate school part-time.

404
405
406
407
408
409
410
411
412
413
414
415



Frank Seifert was born in Berlin, Germany. He received the Dipl.-Ing. and Dr.-Ing. degrees in electrical engineering from the Leibniz University of Hannover, Hannover, Germany, in 2002 and 2009, respectively.

From 2009 to 2012, he was with the California Institute of Technology, Pasadena, CA, USA, where he was involved in the research on the frequency stabilization of lasers for high-precision metrology. He is currently with the National Institute of Standards and Technology, Gaithersburg, MD, USA,

where he is involved in

the research on the Kibble balance.

416
417
418
419
420
421
422
423
424
425
426
427
428



Darine Haddad (M'09) received the Ph.D. degree in optics, optoelectronics, and microwaves from the University of Versailles, Versailles, France, in 2004.

She was with the University of Versailles, where she was involved in teaching and conducting research in the field of optical sensors and dimensional metrology. She was a Post-Doctoral Fellow with the Laboratoire National de Metrologie et d'Essais, Trappes, France, in 2004, and the National Institute of Standards and Technology, Gaithersburg, MD, USA, in 2008, where she was involved in

Kibble balance experiments to measure the Planck constant and realizing mass.



Julian Stirling received the Ph.D. degree from the University of Nottingham, Nottingham, U.K., in 2014, under the supervision of Prof. P. Moriarty.

He joined the National Institute of Standards and Technology (NIST), Gaithersburg, MD, USA, where he was involved in small force instrumentation, including building optomechanical sensors with femtoNewton resolution, and upgrading the NIST electrostatic force balance. In 2016, he joined the Joint Quantum Institute, University of Maryland at College Park, College Park, MD, USA, where he

was involved in measuring the universal constant of gravitation. In 2018, he joined the University of Bath, Bath, U.K., where he developed open-source scientific hardware which can be reproduced in the developing world for a fraction of the cost of proprietary alternatives. He is currently working on the 3-D printed OpenFlexure microscope and developing open-source metrology tools.

429
430
431
432
433
434
435
436
437
438
439
440
441
442
443
444
445

AQ:6



David Newell received the Ph.D. degree in physics from the University of Colorado, Boulder, CO, USA.

He was a National Research Council Post-Doctoral Fellow with the National Institute of Standards and Technology (NIST), Gaithersburg, MD, USA, where he was involved in the Kibble Balance Project. In 1996, he was a Staff Member with NIST. From 2004 to 2010 and since 2018, he has been a Leader of the Fundamental Electrical Measurements Group.

He was involved in measurements for the realization of microscale and nanoscale forces traceable to the International System of Units (SI), helped establish the use of graphene in quantum electrical standards and was involved in the construction of a new Kibble balance to realize the kilogram from a fixed value of the Planck constant.

Dr. Newell is a member of the Philosophical Society of Washington and a Fellow of the American Physical Society. He is the Chair of the CODATA Task Group on Fundamental Constants, which provided the exact values of the fundamental constants that form the foundation of the revised SI.

AQ:7

446
447
448
449
450
451
452
453
454
455
456
457
458
459
460
461
462
463
464



Stephan Schlamminger received the Diploma degree in physics from the University of Regensburg, Regensburg, Germany, in 1998, and the Ph.D. degree in experimental physics from the University of Zurich, Zurich, Switzerland, in 2002. His thesis was on the determination of the Universal Constant of Gravitation.

From 2002 to 2010, he was with the University of Washington, Seattle, WA, USA, where he was involved in the experimental test of the equivalence principle. In 2010, he was with the National Institute of Standards and Technology (NIST), Gaithersburg, MD, USA, where he was involved in Kibble balance. In 2016, he was a Group Leader of the Fundamental Electrical Measurement Group. From 2017 to 2018, he was with the Regensburg University of Applied Science, Regensburg, Germany, where he taught physics. Since 2018, he has been a Physicist with NIST.

465
466
467
468
469
470
471
472
473
474
475
476
477
478
479
480

AUTHOR QUERIES

AUTHOR PLEASE ANSWER ALL QUERIES

PLEASE NOTE: We cannot accept new source files as corrections for your paper. If possible, please annotate the PDF proof we have sent you with your corrections and upload it via the Author Gateway. Alternatively, you may send us your corrections in list format. You may also upload revised graphics via the Author Gateway.

AQ:1 = Please provide the expansion for the acronyms IPK and CAD.

AQ:2 = Author: Please confirm or add details for any funding or financial support for the research of this article.

AQ:3 = The in-text citations of Figs. 6 and 7 are out of order. Please update the in-text citations.

AQ:4 = Please provide the author names, publisher name, and publisher location for Ref. [1].

AQ:5 = Current affiliation in the biographies of Leon Chao, Julian Stirling, and David Newell do not match the First Footnote. Please check and correct where needed.

AQ:6 = Please provide the year of completion when the author David Newell received the Ph.D. degree.

AQ:7 = Please provide the location for Leader of the Fundamental Electrical Measurements Group and Fundamental Electrical Measurement Group.

The Design and Development of a Tabletop Kibble Balance at NIST

Leon Chao[®], Frank Seifert, Darine Haddad, *Member, IEEE*, Julian Stirling, David Newell, and Stephan Schlamminger

Abstract—On November 16, 2018, the 26th General Conference on Weights and Measures voted unanimously to revise the International System of Units from a system built on seven base units to one built on seven defining constants and will officially become effective on May 20, 2019, or World Metrology Day. More specifically, the unit of mass, the kilogram, will be realized via a fixed value of the Planck constant h and a Kibble balance (KB) serves as one method of achieving this. Over the past few decades, national metrology institutes around the world have developed KBs, the majority aimed at realizing the unit of mass at the 1-kg level with uncertainties on the order of a few parts in 10^8 . However, upon fixing the Planck constant, mass can be directly realized at any level, deeming the kilogram only a historically unique benchmark. At the National Institute of Standards and Technology, a tabletop-sized Kibble balance (KIBB-g1) designed to operate at the gram-level range with uncertainties on the order of a few parts in 10^6 is currently under development.

Index Terms—Kibble balance (KB), mass metrology, precision engineering design.

I. INTRODUCTION

THE maximum permitted uncertainties for International Organization of Legal Metrology (OIML) class E₁ calibration weights ranging from 1 to 10 g are on the order of a few micrograms, limited by the accrued uncertainties associated with repeatability of the balances used within the traceability chain to the IPK and the stability of the artifacts [1]. With the revised International System of Units, mass can be directly realized at any scale point (i.e., milligram, gram, kilogram, etc.) [3]. Instrument manufacturers and pharmaceutical companies have shown interest in directly measuring small masses and a tabletop Kibble balance (KB) capable of realizing mass with the same level of uncertainties associated with a set of calibration weights can replace the need for such a set. Operating at this level of relative uncertainty also removes the demand for quantum electrical standards, gravimeters, and high-vacuum environments required in more accurate KBs. Here, as an extension of [2], we describe the design and development of KIBB-g1, or (KIB)ble (B)alance at the (g)ram level, version (1), aimed at achieving uncertainties on the order of a few micrograms. The final results show promise and set

a foundation for future work in generating a full uncertainty budget.

II. THEORY OF A KIBBLE BALANCE

Even though a KB might appear functionally similar to an equal-arm beam balance, a significant difference exists. A conventional beam balance makes relative measurements, comparing the weight an object to that of a calibrated mass. A KB, however, makes absolute measurements, comparing the weight of an object to a frequently calibrated electromagnetic force determined by electrical quantities. The experiment involves two modes of operation, velocity mode, and force mode. Velocity mode is based on the principle of Faraday's law of induction. A coil (wire length L) is moved at a velocity v through a magnetic field (flux density B) so that a voltage V is induced. The induced voltage is related to the velocity through the flux integral BL

$$V = BLv. \quad (1)$$

Force mode is based on Lorentz forces. The gravitational force on a mass m is counteracted by an upward electromagnetic force F generated by the now current-carrying coil in a magnetic field

$$F = BLI = mg \quad (2)$$

where g is the local gravitational acceleration and I is the current in the coil.

By combining (1) and (2), canceling out the BL factor common to both equations, and rearranging the variables, expressions for electrical and mechanical power are equated and a solution for mass is obtained

$$VI = mgv \implies m = \frac{VI}{gv}. \quad (3)$$

The above-mentioned equation relates mechanical power to electrical power and provides a means to relate mass to electrical quantities. The relationship equates “virtual” power, in the sense that the factors of each product, V and I or mg and v , are not measured simultaneously but separately in the two modes. The “power” only exists virtually, i.e., as a mathematical product.

Since KIBB-g1 strives for relative uncertainties on the order of a few parts in 10^6 , the Planck constant only makes a subtle appearance as the means for absolutely calibrating the hardware associated with the electrical quantities.

Manuscript received July 13, 2018; revised December 26, 2018; accepted February 1, 2019. The Associate Editor coordinating the review process was Djamel Allal. (*Corresponding author: Leon Chao.*)

The authors are with the National Institute of Standards and Technology, Gaithersburg, MD 20899 USA (e-mail: leon.chao@nist.gov).

Color versions of one or more of the figures in this paper are available online at <http://ieeexplore.ieee.org>.

Digital Object Identifier 10.1109/TIM.2019.2901550

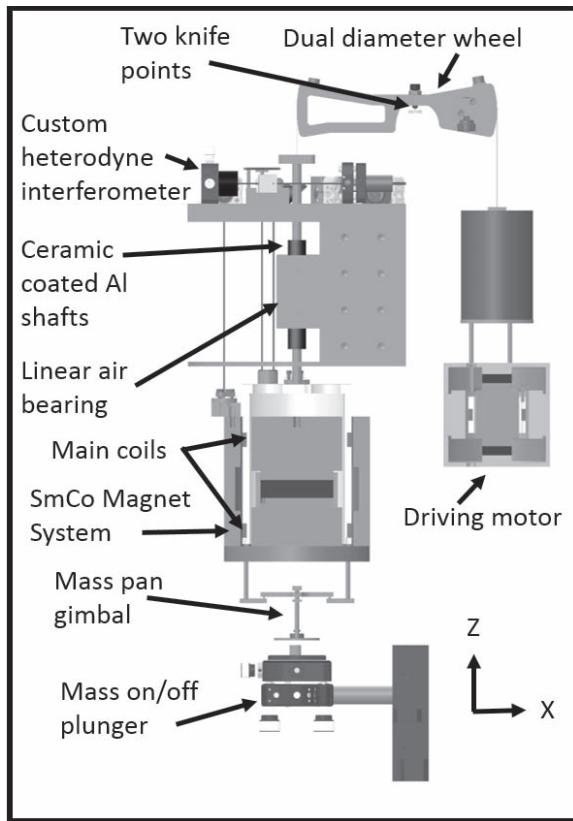


Fig. 1. CAD rendering of the KIBB-g1 KB. Structural components have been hidden for clarity. Cross-sectional views of both magnets/coils are shown. The MMS is everything to the left of the knife points and the CMS to the right.

III. DESIGN OVERVIEW

A. Mechanical

The KIBB-g1 KB was designed with the intention of providing industrial laboratories with the capability to directly realize mass units at the gram level on site. With this in mind, we set out five design goals as follows.

- 1) Form factor: “tabletop” sized instrument.
- 2) Cost: < 50 000 USD.
- 3) Nominal values: between 1 and 10 g.
- 4) Relative uncertainties: $\approx 10^{-6}$.
- 5) Convenience: operates in air (no vacuum required).

KIBB-g1 measures 57 cm tall and 30 cm in diameter and is designed such that the “main mass side” (MMS) contains all the components relevant to velocity and force mode while the “counter mass side” (CMS) serves as a driving motor. For a detailed description of KB theory and design (see [4]).

Starting from the top of the balance as shown in Figs. 1 and 2, a dual-diameter truncated wheel pivots about a two-point contact, essentially forming a line contact, which we will commonly refer to as the “knife points.” The two pivot points are commercially available nonmagnetic Niva Alloy¹ points and each rests on a polished sapphire disk.

¹Certain commercial equipment, instruments, and materials are identified in this paper in order to specify the experimental procedure adequately. Such an identification is not intended to imply recommendation or endorsement by the National Institute of Standards and Technology nor is it intended to imply that the materials or equipment identified are necessarily the best available for the purpose.

The simple design of the two knife points essentially provides a straight line contact without the need for manufacturing a precision knife edge.

The truncated wheel looks like a beam but effectively behaves as a wheel. The prescribed motion of the hanging coils along the z -axis is constrained by the rotation of the wheel about the y -axis. The MMS beam arc has a smooth, curved surface with a radius 1.4 times that of the CMS arc where both arcs are concentric. This radius mismatch allows for increased space on the MMS without increasing the form factor of the entire apparatus. Each knife-point is rigidly attached to the end of a screw inserted through the center of the balance beam. Adjusting the depth of each screw allows aligning the rotational degree of freedom (DOF) about the x -axis and translational DOF in the z -axis. This is critical for adjusting the location of the truncated wheel’s center of gravity as well as aligning its geometric center to the rotation center of the knife points.

The MMS electromagnet system consists of two coils with 3253 turns and mean diameter of 73 mm each wound from magnet wire with a diameter of 0.06 mm. The MMS permanent magnet is comprised of a single SmCo magnet disk, the magnetic flux of which is guided by a mild steel yoke. The system is designed such that the magnetic flux is guided radially through the two air gaps for interaction with the two coils. The magnetic flux density through the air gaps is measured to be about 0.4 T.

The coil is rigidly connected to two parallel ceramic coated aluminum shafts and is suspended from the MMS of the beam via a titanium wire. One of the parallel shafts is guided by an air bearing operating at about 240 kPa above the atmosphere. The original design included air bearings for both shafts but the parallelism alignment proved difficult for overcoming the effects of overconstraining. Two shielding plates were bolted above and below the air bearing to reduce the noise from the exhaust. We conducted a force mode measurement with varying input pressures ranging from 240 to 700 kPa, and through higher pressures resulted in an increase in noise, the overall mass determination for each pressure level was consistent. In principle, the air exhaust is a constant offset force common in both the mass ON and mass OFF states during force mode. A vertical tube is implemented to shield the laser paths from small refractive index fluctuations caused by the exhaust air. The lab temperature, humidity, and pressure fluctuations have been measured by an environmental sensor placed next to the magnet for buoyancy and refractive index corrections and the effect of each contributes relatively less than 1×10^{-6} . Suspended from the bottom of the coil is a mass pan gimbal and a piston loads and unloads the test mass.

The CMS consists of a small coil mounted below a copper tube (a dead mass to account for the mass on the MMS), suspended by two filaments of the same wire as the MMS. Small NdFeB magnets interact with the copper tube and serve as eddy current dampers for suppressing the pendulum modes of the CMS hanging assembly. The CMS coil hangs inside a closed-circuit NdFeB/mild steel magnet system.



Fig. 2. Photograph of KIBB-g1. White hose for air bearing supply.

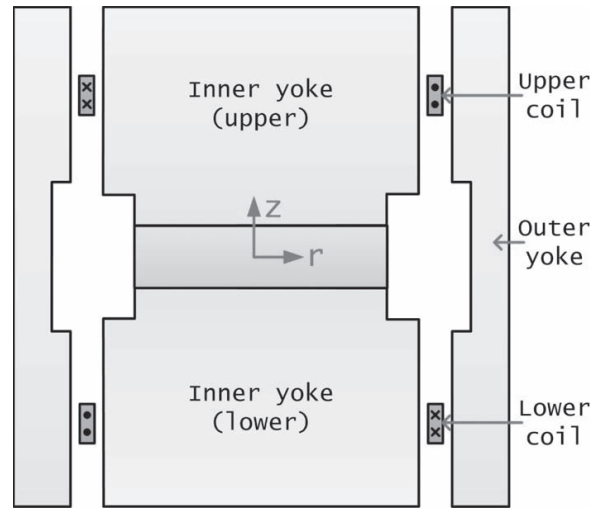


Fig. 3. Cross-sectional representation of the magnet system. Two coils wound on the same former are connected in series opposition. Each coil has 3253 windings. Two halves of the outer yoke have been simplified to a single sleeve.

a PCI-6251 DAQ. In velocity mode, the induced voltage is measured with an Agilent 3458A voltmeter and in force mode, the full voltage drop produced by the weighing current traversing a Fluke 742A 1-k Ω calibrated resistor is measured. All measurement and timing triggers are controlled by a PXI 7831R field-programmable gate array (FPGA). A global positioning system receiver producing a 10-MHz signal serves as the timing source for both the FPGA and TIAs.

161 *B. Optical*

162 A dual frequency 2.83-MHz Zeeman-split laser is used as
 163 the source for the Michelson heterodyne interferometer for
 164 measuring and controlling the displacement of the main coil
 165 along Z . The measurement laser beam of the interferometer
 166 projects onto a flat mirror mounted centered on the top surface
 167 of the coil former adjustable in angle about X and Y . Because
 168 the angular DOF of the coil is constrained by the air bearings,
 169 a simple flat mirror was chosen instead of a retroreflector. The
 170 reference arm projects onto a similar mirror system mounted
 171 to the top edge of the magnet. This location was chosen to
 172 minimize the optical path difference between the two arms and
 173 for common mode rejection of mechanical vibration between
 174 the coil and magnet. The interferometer signals are read
 175 through two Carmel Instruments time interval analyzers (TIA).
 176 One TIA serves as a continuous position and time readout,
 177 whereas the second TIA serves as the measurement readout
 178 for velocity only when triggered. A horizontal displacement
 179 sensor (HDS) is comprised of a separate laser beam which
 180 reflects off a corner cube mounted off-center of the coil former
 181 onto a 2-D position sensor for monitoring minute parasitic
 182 X and Y motions of the coil during the velocity trajectory
 183 and as an aid for aligning the trajectory to gravity.

184 *C. Electrical*

185 The KIBB-g1 coils are connected to a custom built 26-bit
 186 current source through a relay box ultimately controlled by

187 *D. Magnetic*

188 The KIBB-g1 magnet system employs a single SmCo disk
 189 measuring 12.7 mm in height and 50.8 mm in diameter as
 190 the source of the magnetic circuit. Two nearly identical mild
 191 steel cylinders sandwich the magnet and are concentrically
 192 constrained by an aluminum sleeve as shown in Fig. 3. These
 193 three components make up the inner yoke. Two symmetric
 194 tubes made from the same steel are stacked and locked to
 195 each other via three dowel pins and serve as the outer yoke
 196 assembly. Both the inner and outer yoke assemblies are bolted
 197 to an aluminum base plate capable of tip, tilt, and vertical
 198 translation.

199 The upper and lower 7.6-mm-wide and 35.6-mm-tall air
 200 gaps contain the radial magnetic field and are designed to
 201 guide linearly increasing or decreasing magnetic flux densities
 202 with respect to Z as shown in Figs. 4 and 5. Thus, in principle,
 203 the combined magnetic flux density curve is uniform in the
 204 neighborhood of $Z = 0$.

205 The original design of the magnet utilized a monolithic
 206 tube as the outer yoke. However, due to manufacturing and
 207 assembly procedure asymmetries of both the magnet and the
 208 coils, the combined field profile was measured to have a
 209 0.075-Tm/mm slope. A sloped profile, especially at the weigh-
 210 ing position, is undesirable because the mass determinations
 211 are highly sensitive to small deviations about the weighing
 212 position. In attempt to achieve a flat spot in the profile,
 213 a new outer yoke was fabricated as two separate pieces such
 214 as shown in Fig. 3.

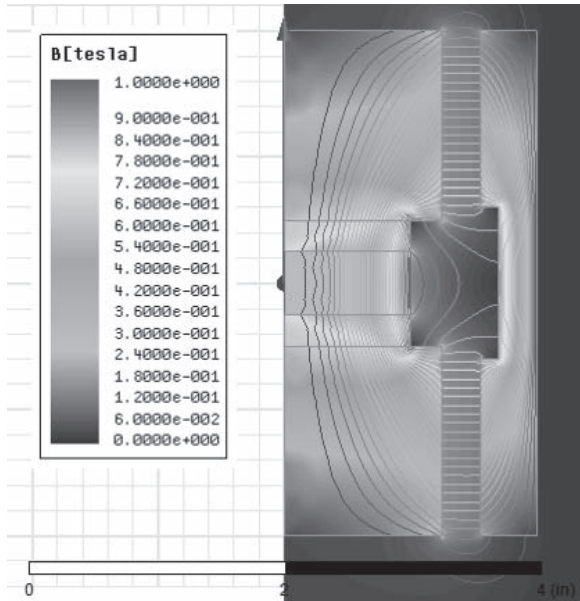


Fig. 4. Finite element simulation of the magnetic flux density through the top and bottom air gaps of half the magnet. The field where the coil resides in weighing mode is approximately 0.4 T.

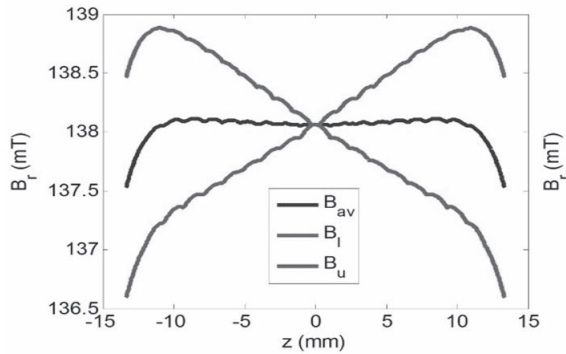


Fig. 5. Theoretical magnetic flux density profile of the upper air gap (B_u), the lower air gap (B_l), and the average of the two (B_{av}) versus vertical position of the coil Z . The MMS coil is comprised of two individual coils connected in series opposition so the measured profile should reflect the shape of B_{av} with a local minimum at $Z = 0$.

that the assembly procedure would be completely symmetric and no yoke pieces would be magnetized more than once. Another attempt was altering the reluctance of the bottom half of the outer yoke with an external magnetic field. Neither attempt influenced the field enough to achieve a uniform profile section. To truly achieve a flat field near $Z = 0$, we had to shim the height of the inner yoke assembly by 2-mm relative to the outer yoke. This led to the most recent magnetic field profile measured in Fig. 7 where the slope is less than 0.004 Tm/mm or in relative terms $2.3 \times 10^{-8}/\mu\text{m}$ near $Z = 0$. The balance controls are typically able to hold weighing position at $Z = 0 \pm 0.5 \mu\text{m}$.

A drawback of the open top/bottom magnet system design is the leakage of the magnetic flux near the unguided regions. Therefore, any test masses will experience a systematic force from the stray magnetic field and its gradient.

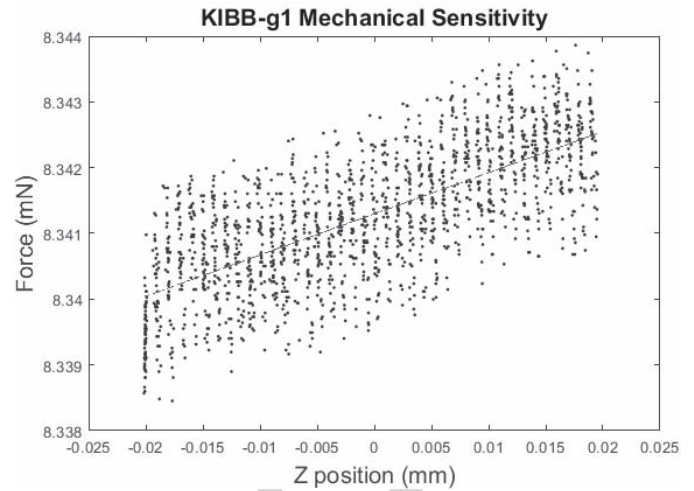


Fig. 6. Measured data of mechanical balance sensitivity between $Z = -0.02 \text{ mm}$ and $Z = 0.02 \text{ mm}$. The force change as a function of Z position is about $0.05 \mu\text{N}/\mu\text{m}$.

The mass pan hangs approximately 50 mm below the bottom surface of the magnet. Thus, for example, an OIML class E₂ 10-g stainless steel mass would experience a force equivalent of a 12-mg mass due to the magnetic susceptibility of the material. A field cancellation procedure of adding a 5-DOF adjustable magnet underneath the mass pan to negate the field at the mass location has proven successful and, in principle, can reduce the magnetic field gradient to zero. However, a strong magnet placed near the mass pan is cumbersome for development purposes so that we have chosen to complete our measurements with masses made from copper for which the systematic forces are negligible.

IV. SYSTEM ALIGNMENT

To align the KB for measurement, verticality of the balance, the HDS, and the interferometer has to be ensured. The magnet, which can be independently tilted, is aligned to be vertical using a precision bubble level. The direction of the interferometer and the HDS laser beams are then aligned to be vertical, defined by g , with reference to an alcohol pool. For example, the verticality of the measurement laser of the interferometer has been adjusted to be within $200 \mu\text{rad}$ mainly due to the length of the optical lever permitted by the depth of the laboratory. The trajectory of the coil is made vertical by iteratively adjusting the KB and HDS to align to g .

At the same time, balance sensitivity was adjusted by shifting the center of gravity of the balance wheel. Two threaded brass masses attached to the CMS of the balance beam allowed to translate in X and Z provide means for such adjustments. Balance sensitivity was adjusted and measured to be about $0.05 \mu\text{N}/\mu\text{m}$ (or $5 \text{ nN}/\mu\text{rad}$ with respect to the wheel angle) near the weighing position, depicted by Fig. 6. As stated earlier, our force mode controller typically holds the position of the coil within $0 \pm 0.5 \mu\text{m}$.

V. MEASUREMENT PROCEDURE AND DATA ANALYSIS

Once the above-mentioned alignment procedure is complete, an acrylic dome is placed over the KB to shield the

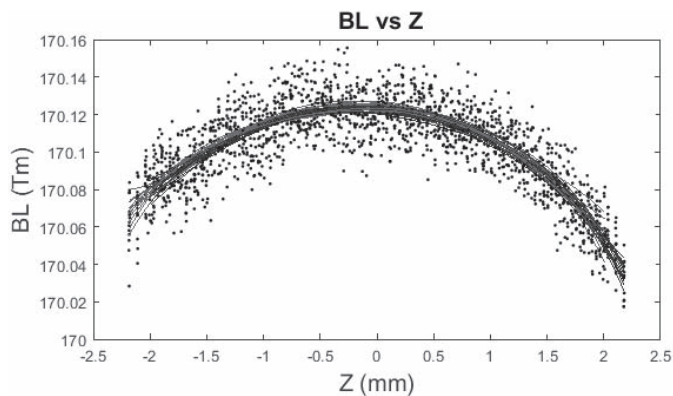


Fig. 7. Example of 29 up/down sweeps superimposed on top of each other in a single-velocity mode data set. BL is plotted against Z position of the coil. Induced voltage is measured at 2 NPLC, 1 mm/s from $Z = -2.2$ mm to $+2.2$ mm. A least squares regression is applied to each sweep.

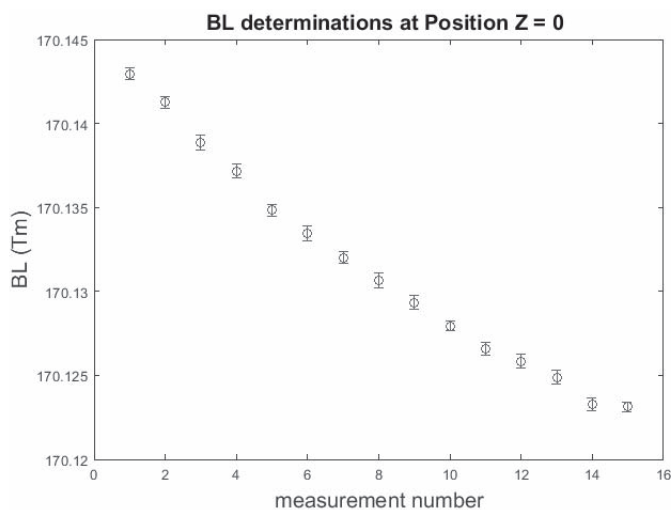


Fig. 8. BL determinations of a full measurement spanning 4.5 h. The relative statistical uncertainty of each determination is on average 2×10^{-6} ($k = 1$). The overlying drift is caused by change of the magnetization due to temperature fluctuations of the laboratory.

274 instrument from air currents caused by the air conditioning in
 275 the laboratory. A small hole in the dome allows passage for the
 276 interferometer laser beam. For the rest of this paper, we will
 277 reference our first attempt at measuring the mass of a copper
 278 cylinder with a value of 10.164780(5) g ($k = 1$, calibrated by
 279 the National Institute of Standards and Technology Mass and
 280 Force Group).

281 Velocity mode operates with the 10-g mass resting on the
 282 mass pan and the KB balanced. The measurement begins
 283 with 14 up and 15 down velocity sweeps with a constant
 284 velocity of 1mm/s while sampling the DVM every 2 power
 285 line cycles (NPLC) or 33 ms. These parameter values were
 286 chosen based on examining the power spectrum of velocity
 287 noise and a separate parametric study between differing NPLC
 288 and velocity values. The FPGA triggers both the sampling of
 289 the TIA and DVM. For example, each voltage measurement
 290 is bracketed by 17 position and time readings where each
 291 set is averaged down to a single position and time. The
 292 velocity during the voltage measurement is determined by
 293 the difference of two consecutive position readings divided
 294 by the sample time. From the voltage and velocity data
 295 pairs, the quotient is calculated, and this is the BL . Each
 296 sweep consists of 60 BL measurements each with its own
 297 Z position ranging between $Z = \pm 2.2$ mm. For this data set,
 298 the least squares regression is performed. Fig. 7 shows the data
 299 of 29 up/down sweeps superimposed on each other. The solid
 300 lines show the polynomial fits. Fig. 8 shows the average of the
 301 BL values extracted from the polynomial fits at $Z = 0$ for
 302 each velocity mode set over the span of 4.5 h. Force mode
 303 measurements occur in between each of these points.

304 After a set of velocity mode measurements, the system
 305 toggles to force mode and the balance is served to $Z = 0$
 306 where the maximum of the BL curve resides. A motorized
 307 translation stage first removes the mass, and the perturbation
 308 due to this process is suppressed with tight control gains.
 309 The balance then undergoes a hysteresis erasing procedure
 310 where the balance follows a decaying sinusoidal trajectory
 311 with an initial amplitude larger than that of the perturbation
 312 caused by the mass removal. This is necessary because the

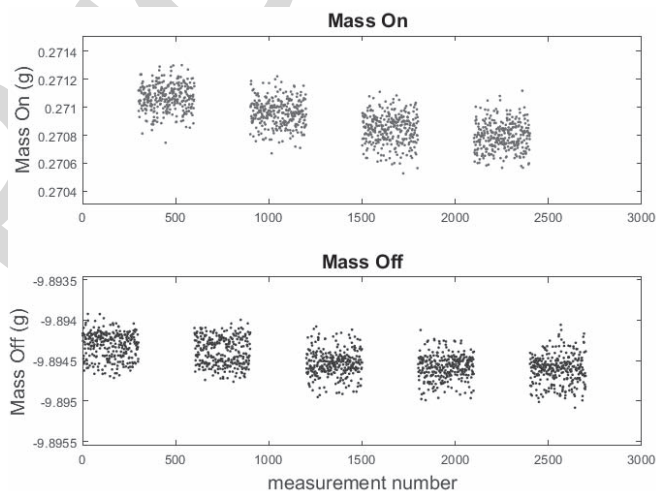


Fig. 9. Example of raw force mode data. Mass imbalance experienced by KIBB-g1 converted from voltage to grams via an interpolated value of BL from bracketing velocity mode measurements is plotted. Four mass on measurements (top). Each cluster is 300 data points taken over 30 s. Five sets of mass off measurements with the same amount of data points and time duration (bottom). The total time required for a weighing mode set is approximately 15 min due to the knife points hysteresis erasing and settling time procedures executed after each mass exchange. Because the distribution seems to have non-Gaussian behavior, we chose not to calculate the standard deviation of the mean for this data set. Thus, all clusters have a relative uncertainty of about 2×10^{-5} ($k = 1$).

313 pivot points are not ideal, frictionless surfaces, and incur a
 314 bias restoring force depending on the direction and amplitude
 315 of the excursion from mass exchanges. Immediately after the
 316 erasing procedure, controller feedback switches to a set of
 317 gains optimized for current noise. After some settling time,
 318 300 current measurements are taken, once every power line
 319 cycle. The process is then repeated for a mass on measurement.
 320 In total, a set of nine mass ON/OFF measurements are taken
 321 per force mode set as shown in Fig. 9. It may be seen that the

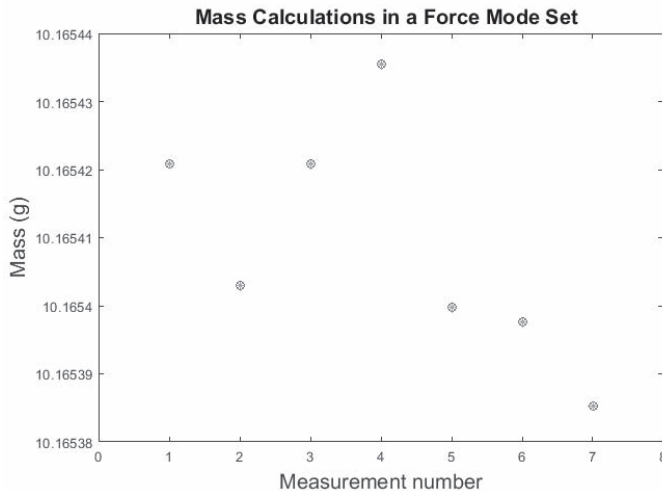


Fig. 10. Example of a set of seven mass calculations in a force mode set. The relative statistical uncertainty of each force mode set is on average 5×10^{-6} ($k = 1$).

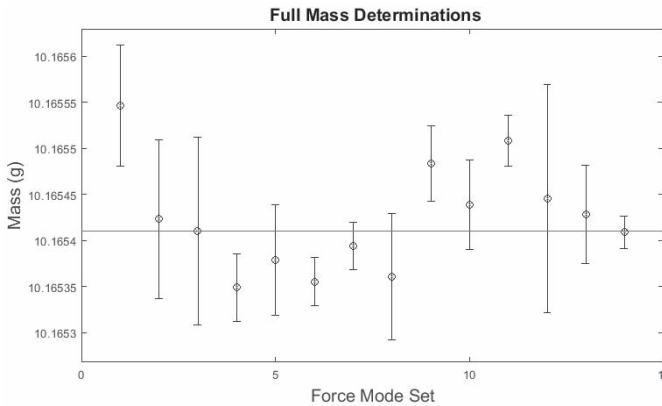


Fig. 11. Example of a set of mass determinations for a copper cylinder with a mass value believed to be 10.164780(5) g. Weighting the data gives a value of 10.16541 g (horizontal line) with a relative statistical uncertainty of 1.2×10^{-6} ($k = 1$). However, the uncertainty needs to be multiplied by an expansion factor of 1.47 (see text).

weighings are asymmetric, that is,

$$|M_{\text{off}}| \neq |M_{\text{on}}|. \quad (4)$$

This is due to mechanical limitations of KIBB-g1, but it is typically best practice to conduct symmetric weighings in a KB experiment.

After the conclusion of the full measurement of 15 velocity mode and 14 force mode sets, the force mode voltage measurements are converted to mass via a linearly interpolated BL value from bracketing velocity mode sets, allowing for seven mass calculations per force mode set as shown in Fig. 10. The first mass calculation is defined as

$$\frac{M_{\text{off}1} - M_{\text{off}2}}{2} - M_{\text{on}1}. \quad (5)$$

The second mass calculation is defined as

$$M_{\text{off}2} - \frac{M_{\text{on}1} - M_{\text{on}2}}{2} \quad (6)$$

and so on. This is to remove any linear time-dependent drift of the magnetic field, usually due to temperature fluctuations, since mass ON and mass OFF are measured at different times. Fig. 9 depicts a typical force mode set. A full measurement set of mass determinations is shown in Fig. 11.

VI. CONCLUSION

KIBB-g1 is still in the prototyping phase. It is an ongoing effort to characterize the apparatus and understand the uncertainties contributing to the accuracy of the measurements. Many of the systematic uncertainties are known to have relative effects at or below 1×10^{-6} , i.e., local acceleration of gravity, laser wavelength, and frequency, refractive index, and buoyancy changes due to environmental fluctuations, resistor, and DVM drift. Temperature, air pressure, and humidity are constantly monitored in the laboratory, and an index of refraction correction for the laser wavelength has been applied. So far, we have been focused on the precision and repeatability of KIBB-g1.

In Fig. 11, 14 data points are represented with their statistical uncertainties. The weighted mean of the data has a relative statistical uncertainty of 1.2×10^{-6} . The χ^2 is 28 for $N - 1 = 13$ DOF, larger than the expected 13. In this case, it is custom to enlarge the individual uncertainties by the Birge ratio, $(\chi^2/(N - 1))^{1/2} = 1.47$. This leads to a relative statistical uncertainty of the mean of 1.7×10^{-6} .

The data in Fig. 11 show a nonstationary pattern. We believe this caused by either choppy mass exchanges or gain changes in the control loop. This is currently under investigation. The pattern in the data is the cause of the larger than expected χ^2 .

The data presented here indicate the precision of KIBB-g1 has uncertainties of about 1.7×10^{-6} on a nominally 10-g mass but the difference between our measured value and the true value is about 6.2×10^{-5} . Thus, we must continue investigating the systematic errors associated with the instrument before an absolute measurement and full uncertainty budget can be completed.

ACKNOWLEDGMENT

The authors would like to thank S. Li for the magnet design, A. Panna for helping with the software development, M. Kraft for the resistor calibration, B. Waltrip and M. Berilla for the current source design, P. Abbott and K. Chesnutwood for the mass calibrations, and J. Pratt and G. Shaw for general support.

REFERENCES

- [1] *Weights of Classes E1, E2, F1, F2, M1, M2, M3, Committee Draft OIML/CD R 111-1 of Edition*, 2004.
- [2] L. Chao, F. Seifert, D. Haddad, S. Schlamminger, "The design and development of a tabletop Kibble balance at NIST," in *Proc. Conf. Precis. Electromagn. Meas.*, Jul. 2018, pp. 1–3.
- [3] D. Haddad *et al.*, "Measurement of the Planck constant at the National Institute of Standards and Technology from 2015 to 2017," *Metrologia*, vol. 54, pp. 633–641, Jul. 2017.
- [4] I. A. Robinson and S. Schlamminger, "The watt or Kibble balance: A technique for implementing the new SI definition of the unit of mass," *Metrologia*, vol. 53, pp. 46–74, Sep. 2016.
- [5] D. Haddad *et al.*, "A precise instrument to determine the Planck constant, and the future kilogram," *Rev. Sci. Instrum.*, vol. 87, May 2016, Art. no. 061301.

336
337
338
339
340
341
342
343
344
345
346
347
348
349
350
351
352
353
354
355
356
357
358
359
360
361
362
363
364
365
366
367
368
369
370
371
372
373
374
375
376
377
378
379
380
381
382
383
384
385
386
387
388
389
390
391
392

AQ:5
393
394
395
396
397
398
399
400
401
402
403



Leon Chao received the B.S. degree in mechanical engineering from the University of Maryland at College Park, College Park, MD, USA, in 2012.

In 2012, he joined the Fundamental Electrical Measurements Group, National Institute of Standards and Technology, Gaithersburg, MD, USA, as a Mechanical Engineer. He is currently with the University of Maryland at College Park, where he is involved in two Kibble balance experiments, NIST-4 and KIBB-g1, while attending graduate school part-time.

404
405
406
407
408
409
410
411
412
413
414
415



Frank Seifert was born in Berlin, Germany. He received the Dipl.-Ing. and Dr.-Ing. degrees in electrical engineering from the Leibniz University of Hannover, Hannover, Germany, in 2002 and 2009, respectively.

From 2009 to 2012, he was with the California Institute of Technology, Pasadena, CA, USA, where he was involved in the research on the frequency stabilization of lasers for high-precision metrology. He is currently with the National Institute of Standards and Technology, Gaithersburg, MD, USA,

where he is involved in

the research on the Kibble balance.

416
417
418
419
420
421
422
423
424
425
426
427
428



Darine Haddad (M'09) received the Ph.D. degree in optics, optoelectronics, and microwaves from the University of Versailles, Versailles, France, in 2004.

She was with the University of Versailles, where she was involved in teaching and conducting research in the field of optical sensors and dimensional metrology. She was a Post-Doctoral Fellow with the Laboratoire National de Metrologie et d'Essais, Trappes, France, in 2004, and the National Institute of Standards and Technology, Gaithersburg, MD, USA, in 2008, where she was involved in

Kibble balance experiments to measure the Planck constant and realizing mass.



Julian Stirling received the Ph.D. degree from the University of Nottingham, Nottingham, U.K., in 2014, under the supervision of Prof. P. Moriarty.

He joined the National Institute of Standards and Technology (NIST), Gaithersburg, MD, USA, where he was involved in small force instrumentation, including building optomechanical sensors with femtoNewton resolution, and upgrading the NIST electrostatic force balance. In 2016, he joined the Joint Quantum Institute, University of Maryland at College Park, College Park, MD, USA, where he

was involved in measuring the universal constant of gravitation. In 2018, he joined the University of Bath, Bath, U.K., where he developed open-source scientific hardware which can be reproduced in the developing world for a fraction of the cost of proprietary alternatives. He is currently working on the 3-D printed OpenFlexure microscope and developing open-source metrology tools.

429
430
431
432
433
434
435
436
437
438
439
440
441
442
443
444
445

AQ:6

AQ:7



David Newell received the Ph.D. degree in physics from the University of Colorado, Boulder, CO, USA.

He was a National Research Council Post-Doctoral Fellow with the National Institute of Standards and Technology (NIST), Gaithersburg, MD, USA, where he was involved in the Kibble Balance Project. In 1996, he was a Staff Member with NIST. From 2004 to 2010 and since 2018, he has been a Leader of the Fundamental Electrical Measurements Group.

He was involved in measurements for the realization of microscale and nanoscale forces traceable to the International System of Units (SI), helped establish the use of graphene in quantum electrical standards and was involved in the construction of a new Kibble balance to realize the kilogram from a fixed value of the Planck constant.

Dr. Newell is a member of the Philosophical Society of Washington and a Fellow of the American Physical Society. He is the Chair of the CODATA Task Group on Fundamental Constants, which provided the exact values of the fundamental constants that form the foundation of the revised SI.

446
447
448
449
450
451
452
453
454
455
456
457
458
459
460
461
462
463
464



Stephan Schlamminger received the Diploma degree in physics from the University of Regensburg, Regensburg, Germany, in 1998, and the Ph.D. degree in experimental physics from the University of Zurich, Zurich, Switzerland, in 2002. His thesis was on the determination of the Universal Constant of Gravitation.

From 2002 to 2010, he was with the University of Washington, Seattle, WA, USA, where he was involved in the experimental test of the equivalence principle. In 2010, he was with the National Institute of Standards and Technology (NIST), Gaithersburg, MD, USA, where he was involved in Kibble balance. In 2016, he was a Group Leader of the Fundamental Electrical Measurement Group. From 2017 to 2018, he was with the Regensburg University of Applied Science, Regensburg, Germany, where he taught physics. Since 2018, he has been a Physicist with NIST.

465
466
467
468
469
470
471
472
473
474
475
476
477
478
479
480